

Beam separating with the zeroth order eliminated by sandwiched grating

XIAOQING ZHU, BO WANG*, JIAHAO LI, XIAOFENG WANG, HONG ZOU, LIQUN LIU, LINJIAN HUANG, XU YANG, WEIYI YU, JINHAI HUANG

School of Physics and Optoelectronic Engineering, Guangdong University of Technology, Guangzhou 510006, China

In this paper, a two-port encapsulated grating with a connecting layer is demonstrated, which can suppress 0th order under the condition of normal incidence. When the incident light wavelength is 800 nm, the diffraction efficiencies of ± 1 st orders exceed 44% and that of 0th order is less than 3% under transverse electric and transverse magnetic polarizations. In addition, the fabrication tolerance of the grating is also brilliant. In the period range of 1541-1632 nm and the duty cycle of 0.27-0.36, the diffraction efficiencies of ± 1 st orders can reach more than 42%. In this paper, the parameters of the grating are optimized by rigorous coupled-wave analysis. Furthermore, the results show that the proposed grating has important application in optical communication, optical storage, etc.

(Received July 16, 2021; accepted October 5, 2022)

Keywords: Sandwiched grating, Two-port output, Elimination of the zeroth order, Beam splitter

1. Introduction

With the increasing demand for highly integrated optoelectronic devices and the growing maturity of semiconductor processing technology, subwavelength gratings [1-3] have attracted more and more attention in the industry due to their high adaptability to integration. Therefore, the study of multi-functional beam splitter [4-6] based on subwavelength grating structure has strong theoretical significance and practical value. As an important optical device, power splitter [7, 8] which refers to the optical device that can equally distribute the energy of the incident light to the output direction is widely used in various optical systems. The power splitter which can average the energy of the incident light into two output directions is called two-port splitter [9-11]. In recent years, two-port grating have been extensively researched. *Wang et al.* proposed a low-contrast transmission grating and a mixed metal reflective grating under normal incidence [9]. *Fu et al.* designed a two-port reflective grating with a connecting layer [8]. *Yin et al.* proposed a two-port metal-dielectric grating under normal incidence at the incident wavelength of 800 nm [11].

The vector diffraction theory of grating includes finite element method (FEM) [12-14], rigorous coupled-wave analysis (RCWA) [15-19], etc. Among them, RCWA can analyze the relationship between the upper and lower boundary surface electromagnetic fields in terms of eigenvalue and eigenfield expressions, which is characterized by high speed and efficiency in the calculation process. In addition, the simulated annealing

(SA) algorithm [20, 21] is extremely searchable and does not fall into local optimum solutions. In this paper, the optimization of the grating is based on RCWA and SA. Also, the electric field distribution of the grating is calculated by FEM to better understand the performance of the grating as well as to verify the calculation results.

In this work, a two-port encapsulated grating with ultra-stable and high efficiency is designed by RCWA and SA. For one thing, the proposed grating can uniformly couple the energy of the incident light to ± 1 st orders under transverse electric (TE) and transverse magnetic (TM) polarizations, and both have diffraction efficiencies in excess of 44%. For another, the efficiency of 0th order is suppressed very well, less than 3% at TE and TM polarizations. In addition, the target grating has good bandwidth and process tolerance. Such a grating has very important value in the field of optical components [22, 23], optical communication [24-26] and optical systems [27-29].

2. Physical design and numerical calculation

The structure of two-port grating with the elimination of the zeroth order is displayed in the Fig. 1. As shown in the Fig. 1, the plane wave enters the grating from the air with the incident angle $\theta=0^\circ$. The grating is made up of four units, the covering layer, grating layer (including grating ridge and grating groove), connecting layer and grating substrate. The covering layer, grating ridge and connecting layer are composed of resin material [30],

whose refractive index is $n_2=1.51$. h_2 is the depth of grating groove, whose refractive index $n_1=1.00$, and the material of grating groove is air. h_1 and h_3 are the thicknesses of the covering layer and connecting layer, respectively. Material of the grating substrate is Ta_2O_5 with refractive index $n_3=2.00$. In addition, d represents the grating period, w represents the width of the grating ridge, and f represents the duty cycle (defined as $f=w/d$).

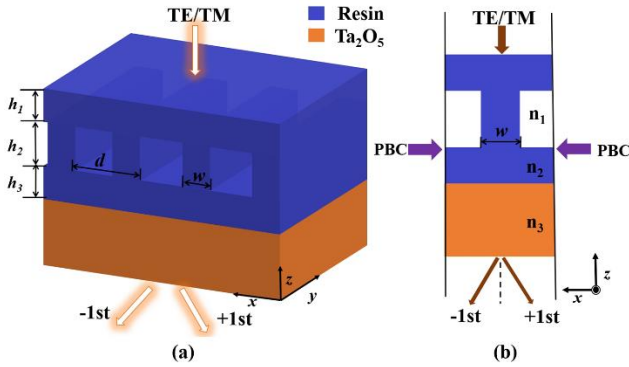


Fig. 1. Schematic of a two-port encapsulated grating under normal incidence: (a) 3-D view (b) sectional view (color online)

In order to complete the calculation of diffraction efficiency (DE), fast screening and optimization of grating parameters, numerical methods such as RCWA and SA are used in the theoretical modelling and numerical optimization process. RCWA obtains the diffraction efficiency of each order by rigorously solving Maxwell's equations in the grating region. A period of grating is selected as the target, and periodic boundary conditions are set in the vertical direction of x -axis. The efficiency of each diffraction order can be obtained by combining the boundary conditions in the transmission region. The specific calculation process can be viewed from Ref. [15]. In addition, the SA algorithm combines the jump characteristics of probability to randomly find the global optimal solution of the objective function in the solution space. Because of the normal incidence, the diffraction efficiencies are the same at ± 1 st orders. To achieve the two-port output with elimination of the zero order, the objective function of the SA algorithm is as follows:

$$\varphi(d, f, h_1, h_2, h_3) = (1 - 2DE_{TE(-1)})^2 + (1 - 2DE_{TM(-1)})^2, \quad (1)$$

where $DE_{TE(-1)}$ and $DE_{TM(-1)}$ are the diffraction efficiencies of -1st order under TE polarization and TM polarization, respectively. The optimized parameters of the grating are finally obtained as $d=1590$ nm, $f=0.3$, $h_1=800$ nm, $h_2=900$ nm and $h_3=700$ nm. Meanwhile, $DE_{TE(-1)}=48.63\%$ and $DE_{TM(-1)}=44.30\%$ are diffracted under these parameters. Compared with Ref. [9], the diffraction efficiencies of the proposed grating at ± 1 st orders for both two polarizations have been significantly improved. The comparative data

with Ref. [9] are shown in Table 1.

Table 1. Comparison of efficiencies between this work and reported Ref. [9]

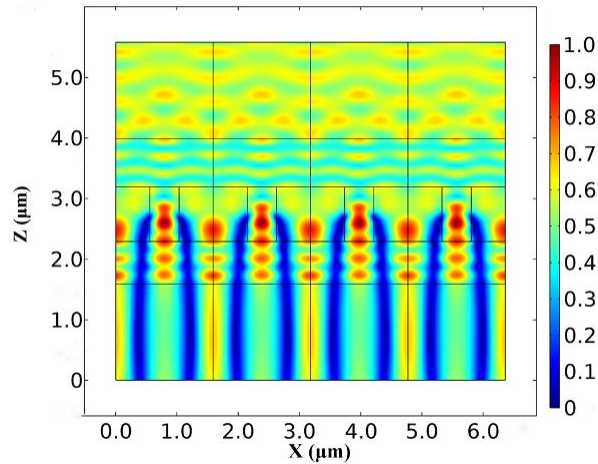
Scheme	η_0^{TE} (%)	$\eta_{\pm 1}^{\text{TE}}$ (%)	η_0^{TM} (%)	$\eta_{\pm 1}^{\text{TM}}$ (%)
Ref. [9]	<1.3%	46.15%	<1.3%	43.60%
This work	0.25%	48.63%	2.90%	44.30%

In addition, from reading Ref. [31] it is known that the modal method uses the modes of a periodic planar waveguide as grating modes, providing a clear physical understanding of the diffraction process. Under normal incidence, only a few grating modes play a dominant role in the diffraction process when the grating period matches the incident wavelength (i.e., when the ratio of grating period to wavelength is between 1-2, the grating has only three output diffraction orders, i.e., 0th and ± 1 st orders). Thus the diffraction process is better understood. The method solves the dispersion equation, calculates the energy exchange between the incident wave and the grating modes, expresses the field at the incident interface in equations and the detailed derivation of the diffraction efficiency of each diffraction order. The results show that the diffraction efficiency of the 0th transmission order is 0, which can be used as a criterion for the 0th order null phase mask, from which approximate grating parameters can also be obtained. The detailed calculation procedure can be viewed in the references.

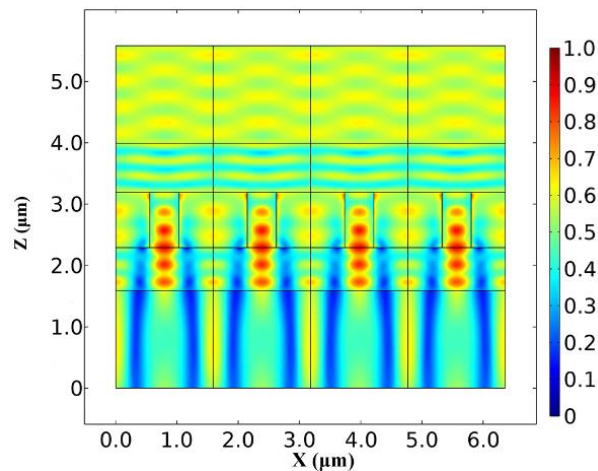
In order to better understand the physical process of light propagation in encapsulated grating and verify the calculation results of RCWA, the diffraction efficiency (listed in Table 2) and electric field distribution under optimum grating parameters are calculated by FEM. Fig. 2 shows the diagram of the normalized electric field distribution of the beam splitting grating at both polarizations. As can be clearly seen from Fig. 2 that the energy distributes from the grating surface to the substrate under the normal incidence of light wavelength of 800 nm. The two electric field distributions also describe the beam splitting effect under TE and TM polarizations, respectively. Due to the periodic structure of the grating, the energy distribution inside the grating also presents the characteristics of periodic. And due to the normal incidence of light waves, the propagation process of incident light and diffractive light present the characteristics of wave along the z -axis. Under the TE and TM polarizations, the location of energy distribution is the same, whereas the TE polarization energy is stronger.

Table 2. The efficiencies of two-port encapsulated grating with the optimized parameters based on RCWA and FEM

Calculation method	η_0^{TE} (%)	$\eta_{\pm 1}^{\text{TE}}$ (%)	η_0^{TM} (%)	$\eta_{\pm 1}^{\text{TM}}$ (%)
RCWA	0.25%	48.63%	2.90%	44.30%
FEM	0.25%	48.66%	2.90%	44.33%



(a)



(b)

Fig. 2. Normalized electric field distribution diagram of the encapsulated grating under normal incidence:
 (a) TE polarization (b) TM polarization (color online)

3. Analysis and discussions

The fabrication process of the target grating in this paper can be proven indirectly by several reported papers. The grating has certain process tolerance in the process of etching [32-35], which needs to be considered in practical application. Fig. 3 shows the equivalent figure of the thickness of the covering layer, the depth of the grating groove and the diffraction efficiency under normal incidence. As shown in Fig. 3, when the thickness of the covering layer $h_1=800$ nm and the depth of the grating

groove $h_2=900$ nm, the diffraction efficiencies of TE polarization at ± 1 st orders and 0th order are 48.63% and 0.25%, and the total efficiency is 97.51%. Under the TM-polarized light wave, the efficiencies of ± 1 st orders are 44.30%, the efficiency of 0th order is 2.90%, and the total efficiency is 91.50%. When the thickness of h_1 is 800 nm and the thickness of h_2 is between 850 nm and 1000 nm, the efficiencies of TE and TM polarizations at ± 1 st orders are better than 44%, and the efficiencies of TE and TM polarizations at 0th order are less than 0.3% and 3%, respectively.

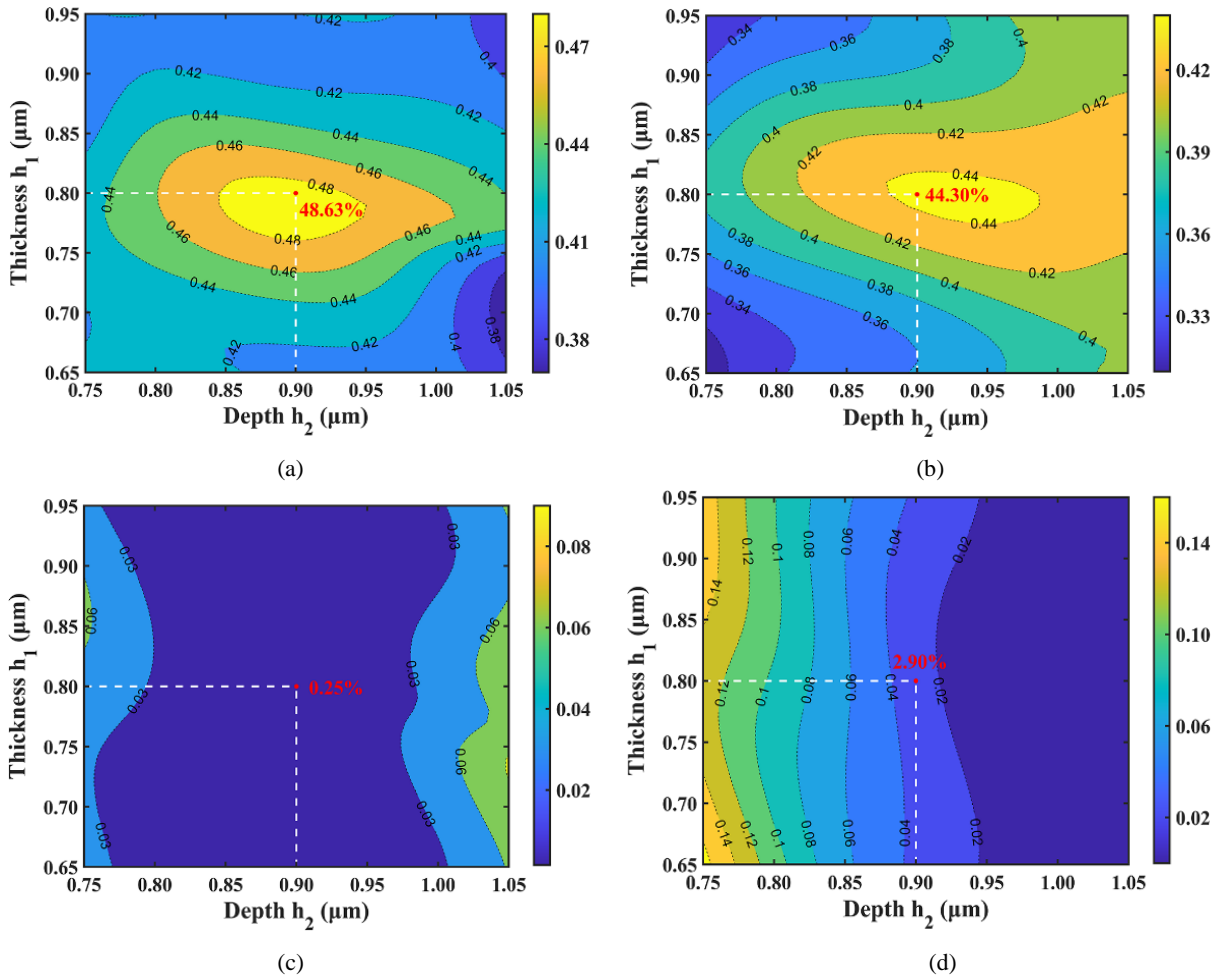


Fig. 3. The efficiency versus the thickness of the covering layer and the grating groove depth under normal incidence with $\lambda=800$ nm, $d=1590$ nm, $h_3=700$ nm and $f=0.3$: (a) 1st order of TE polarization, (b) 1st order of TM polarization, (c) 0th order of TE polarization, (d) 0th order of TM polarization (color online)

Further, Fig. 4 shows a plot of the thickness of the connecting layer h_3 (studied in the range 650-750 nm) versus diffraction efficiency. The results of this plot are based on the condition of normal incidence of 800 nm incident light with $h_1=800$ nm and $h_2=900$ nm. As can be seen, the 0th order is well suppressed at both polarizations, while the diffraction efficiencies of the ± 1 st orders exceed 40% in the studied range.

Based on the optimization results of h_1 , h_2 and h_3 , Table 3 below summarizes the fabrication errors of the three structural parameters for which the diffraction efficiencies are greater than 44% at the ± 1 st orders at both polarizations.

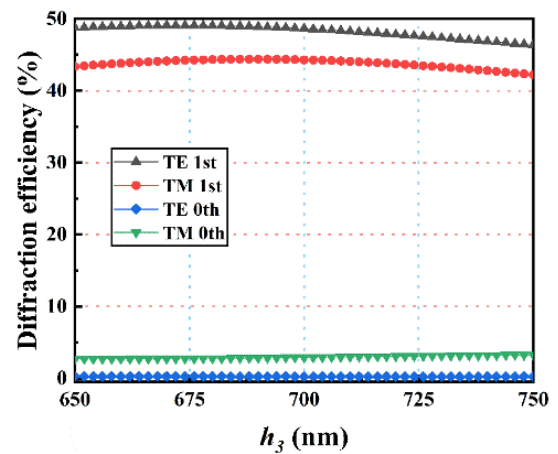


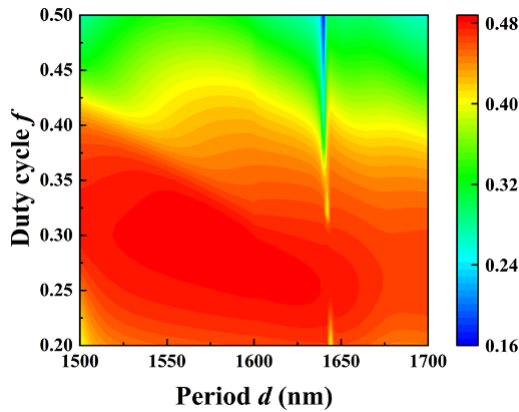
Fig. 4. The relationship between efficiency and h_3 for both two polarizations under normal incidence with $d=1590$ nm, $f=0.3$, $h_1=800$ nm and $h_2=900$ nm (color online)

As can be seen from Table 3, the tolerances of the three structural parameters are all above 45 nm. Particularly for h_2 , the range of diffraction efficiencies greater than 44% at ± 1 st orders for both polarizations are 90 nm. Thus, it can be seen that the three structural parameters (h_1 , h_2 and h_3) of the target structure have good process tolerances.

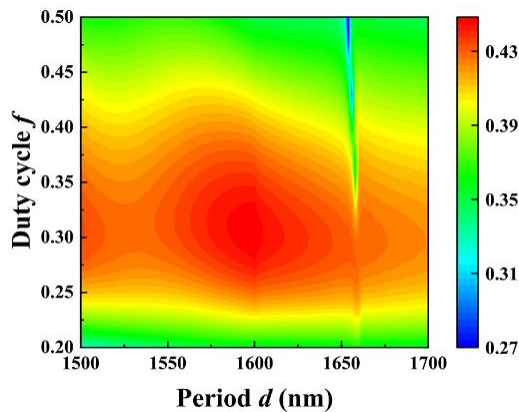
Table 3. Fabrication errors of h_1 , h_2 and h_3

$DE_{TE(-1)}/DE_{TM(-1)}$	Fabrication errors		
	h_1	h_2	h_3
>44%	770-820 nm (50 nm)	890-980 nm (90 nm)	666-712 nm (46 nm)

Next, Fig. 5 shows the diffraction efficiency as a function of the period and duty cycle. It can be seen from Fig. 5 that when the period is 1541-1632 nm and the duty cycle is 0.27-0.36, the ± 1 st orders diffraction efficiencies of TE and TM polarizations are more than 42%.



(a)



(b)

Fig. 5. The diffraction efficiency as a function of the period and duty cycle under normal incidence with $h_1=800$ nm, $h_2=900$ nm, $h_3=700$ nm and $\lambda=800$ nm: (a) 1st order of TE polarization, (b) 1st order of TM polarization (color online)

Under the normal incidence, the optimized grating can achieve the best performance at the wavelength of 800 nm. In practice, however, the central wavelength may drift away from 800 nm. Fig. 6 shows the diffraction efficiencies of the grating at different wavelengths. As depicted here in Fig. 6, the diffraction efficiencies of ± 1 st orders under TE and TM polarizations are higher than 42% in the wavelength range of 775-813 nm, with the bandwidth of 38 nm. In this wavelength bandwidth, the diffraction efficiencies of the 0th order under both TE and TM polarizations are well suppressed at less than 5%. This indicates that the target grating has good performance and good stability, which is of great application value for the practical application of optical elements that need to adjust the wavelength.

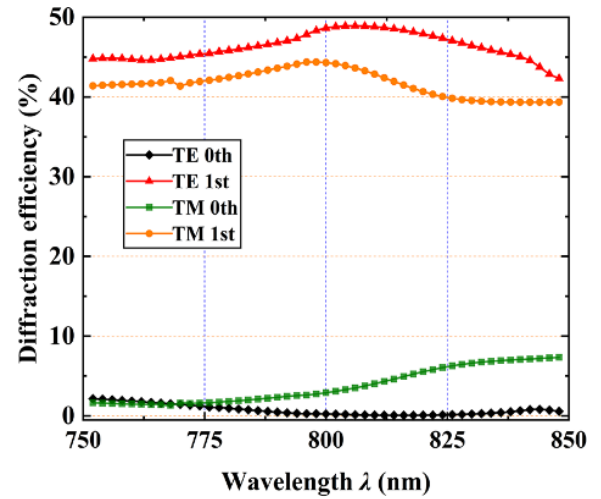


Fig. 6. The relationship between efficiency and incident wavelength for both two polarizations under normal incidence with $d=1590$ nm, $f=0.3$, $h_1=800$ nm, $h_2=900$ nm and $h_3=700$ nm (color online)

In this paper, the condition of incidence angle is normal incidence. However, tolerance of incidence angle should also be taken into account. When the incident angle deviates from 0° (not normal incidence), the diffraction efficiency of +1st order and -1st order will no longer be equal. Fig. 7 shows the diffraction efficiency as a function of the incident angle under the optimum structure. As depicted here in Fig. 7, the diffraction efficiency of the six diffraction orders changed significantly with the deviation of incident angle. However, the diffraction efficiency of ± 1 st orders under two polarizations is higher than 40% at an angular bandwidth of 3.2° , from -1.6° to 1.6° . In this angular bandwidth, the diffraction efficiency at 0th order is well suppressed by less than 4% for both TE and TM polarizations.

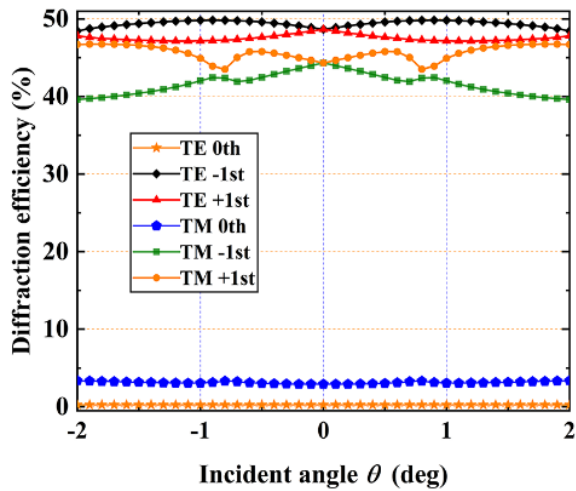


Fig. 7. The diffraction efficiency as a function of the incident angle under the optimum structure (color online)

4. Conclusion

To summarize, an ultra-stable and high-efficiency two-port encapsulated grating with a wavelength of 800 nm at normal incidence is designed. The structural parameters of the grating are analyzed and calculated by RCWA and SA. The proposed grating can complete two-port high-efficiency output at ± 1 st orders under TM and TE polarizations and suppress 0th order. The efficiencies of TE polarization at ± 1 st orders and 0th order are 48.63% and 0.25%, respectively. Under TM-polarized light, the efficiencies of ± 1 st orders are 44.30% in both cases, and the efficiency of 0th order is 2.90%. This shows that the encapsulated grating has a good elimination effect on 0th order. Moreover, the analysis shows that the proposed grating not only can obtain large bandwidth but also have good process tolerance, so as to be applied to more optical components and fields.

Acknowledgements

This work is supported by the Science and Technology Program of Guangzhou (202002030284, 202007010001).

References

- [1] S. Bao, G. Zheng, Y. Ma, *Opt. Mater.* **108**, 110431 (2020).
- [2] W. Xing, D. Zhang, L. Zhang, S. Zhang, Y. Huang, J. Li, A. Guo, W. Li, F. Zhao, *Opt. Mater.* **120**, 111467 (2021).
- [3] G. G. Zheng, P. Zhou, Y. Y. Chen, *Opt. Mater.* **99**, 109581 (2020).
- [4] Z. Huang, B. Wang, Z. Lin, K. Wen, Z. Meng, F. Zhang, Z. Nie, X. Xing, L. Chen, L. Lei, J. Zhou, *Optik* **242**, 167289 (2021).
- [5] A. Zaltron, M. Merano, G. Mistura, C. Sada, F. Seno, *Eur. Phys. J. Plus* **135**(11), 896 (2020).
- [6] J. F. G. Santos, C. H. S. Vieira, *Eur. Phys. J. Plus* **136**(3), 323 (2021).
- [7] Z. Z. Guo, J. B. Xiao, *Opt. Commun.* **488**, 126850 (2021).
- [8] C. Fu, B. Wang, J. M. Fang, K. H. Wen, Z. M. Meng, Q. Wang, Z. G. Nie, X. J. Xing, L. Chen, L. Lei, J. Y. Zhou, *Optoelectron. Adv. Mat.* **14**(7-8), 297 (2020).
- [9] B. Wang, *Sci. Rep.* **5**, 16501 (2015).
- [10] Z. Yin, Y. Lu, J. Yu, C. Zhou, *Chin. Opt. Lett.* **18**(7), 070501 (2020).
- [11] W. H. Zhu, B. Wang, K. H. Wen, Z. M. Meng, Z. G. Nie, X. J. Xing, L. Chen, L. Lei, J. Y. Zhou, *Optik* **202**, 163503 (2020).
- [12] Q. Zhao, W. Yu, Y. Zhao, S. Dai, J. Liu, *Opt. Commun.* **475**, 126282 (2020).
- [13] M. A. Butt, S. N. Khonina, N. L. Kazanskiy, *Wave Random Complex* **31**(1), 146 (2021).
- [14] Y. Kaya, A. Polat, T. Ş. Özşahin, *Eur. Phys. J. Plus* **135**(1), 89 (2020).
- [15] M. G. Moharam, D. A. Pommet, E. B. Grann, T. K. Gaylord, *J. Opt. Soc. Am. A* **12**(5), 1077 (1995).
- [16] S. Y. Wang, G. G. Zheng, F. L. Xian, D. D. Xu, X. M. Hua, *Optik* **231**, 166460 (2021).
- [17] X. D. Du, H. X. Da, *Opt. Commun.* **483**, 126606 (2021).
- [18] W. C. Liu, G. Jin, Y. F. Xie, P. Sun, B. Zhou, W. Jia, J. Wang, C. H. Zhou, *Opt. Commun.* **488**, 126864 (2021).
- [19] B. W. Gong, H. Y. Wen, H. T. Li, *IEEE Photon. J.* **12**(2), 6500208 (2020).
- [20] M. Y. Ou, L. Liu, Y. Liu, L. L. Lan, S. W. Xie, X. T. Shi, *Optik* **225**, 165722 (2021).
- [21] J. Wu, C. H. Zou, H. C. Cao, A. D. Hu, J. J. Yu, W. T. Sun, W. Jia, *J. Opt.* **13**, 115703 (2011).
- [22] X. Y. Liu, Y. Liu, C. Z. Fang, G. Q. Han, Y. Hao, *IEEE Photon. J.* **12**(1), 4800112 (2020).
- [23] R. Nazempour, Q. Y. Zhang, C. B. Liu, X. Sheng, *IEEE Photon. J.* **12**(6) 4200107 (2020).
- [24] M. Q. Wang, S. Q. Lou, *Opt. Commun.* **480**, 126487 (2021).
- [25] Z. X. Cai, T. Shen, W. W. Zhang, J. H. Zheng, *Opt. Commun.* **484**, 126675 (2021).
- [26] C. M. Huang, E. Wijanto, S. P. Tseng, Y. H. Liu, Y. T. Luo, H. C. Lin, H. C. Cheng, *Opt. Commun.* **486**, 126778 (2021).
- [27] P. Nandini, V. Chakravartula, D. Samiappan, R. Kumar, *Optik* **228**, 166215 (2021).
- [28] S. J. Niu, S. T. Wang, M. Ababaik, T. Yusufu, K. Miyamoto, T. Omatsu, *Laser Phys. Lett.* **17**(4), 045402 (2020).
- [29] S. Dewra, R. S. Kaler, *Optoelectron. Adv. Mat.* **14**(1-2), 23 (2020).

-
- [30] Q. Zheng, J. Zhou, Q. Chen, L. Lei, K. Wen, Y. Hu, *IEEE Photon. J.* **11**(6), 2400410 (2019).
- [31] W. T. Sun, P. Lv, C. H. Zhou, J. Wu, S. Q. Wang, *Chin. Opt. Lett.* **11**(7), 070502 (2013).
- [32] X. Mu, Z. M. Chen, L. R. Cheng, S. L. Wu, A. Pepe, X. Tu, H. Y. Fu, *Opt. Commun.* **482**, 126562 (2021).
- [33] Y. Zheng, X. Kai, P. Gao, J. Duan, *Optik* **201**, 163490 (2020).
- [34] S. Yang, J. Xu, Y. Li, L. Wu, X. Quan, L. Fu, M. Liu, X. Cheng, *Opt. Mater.* **118**, 111229 (2021).
- [35] W. F. Jiang, T. Li, J. Y. Miao, L. H. Ma, *Opt. Commun.* **459**, 124887 (2020).

*Corresponding author: wangb_wsx@yeah.net